SCIENCE CHINA
Earth Sciences

• RESEARCH PAPER •

January 2016 Vol.59 No.1: 170–184
doi: 10.1007/s11430-015-5118-2

Heterogeneity in supraglacial debris thickness and its role in glacier mass changes of the Mount Gongga

ZHANG Yong[1,2*], HIRABAYASHI Yukiko[2], FUJITA Koji[3], LIU ShiYin[1] & LIU Qiao[4]

[1] *State Key Laboratory of Cryospheric Sciences, Cold and Arid Regions Environmental and Engineering Research Institute, Chinese Academy of Sciences, Lanzhou 730000, China;*
[2] *Institute of Engineering Innovation, The University of Tokyo, Tokyo 113-8656, Japan;*
[3] *Graduate School of Environmental Studies, Nagoya University, Nagoya 464-8601, Japan;*
[4] *Institute of Mountain Hazards and Environment, Chinese Academy of Sciences, Chengdu 610041, China*

Received March 13, 2015; accepted May 4, 2015; published online September 18, 2015

Abstract In the Tibetan Plateau, many glaciers have extensive covers of supraglacial debris in their ablation zones, which affects glacier response to climate change by altering ice melting and spatial patterns of mass loss. Insufficient debris thickness data make it difficult to analyze regional debris-cover effects. Maritime glaciers of the Mount Gongga have been characterized by a substantial reduction in glacier area and ice mass in recent decades. The thermal property of the debris layer estimated from remotely sensed data reveals that debris-covered glaciers are dominant in this region, on which the proportion of debris cover to total glacier area varies from 1.74% to 53.0%. Using a physically-based debris-cover effect assessment model, we found that although the presence of supraglacial debris has a significant insulating effect on heavily debris-covered glaciers, it accelerates ice melting on ~10.2% of total ablation zone and produces rapid wastage of ~25% of the debris-covered glaciers, leading to the similar mass losses between the debris-covered and debris-free glaciers. Widespread debris cover also facilitates the development of active terminus regions. Regional differences in debris-cover effects are apparent, highlighting the importance of debris cover for understanding glacier mass changes in the Tibetan Plateau and other mountain ranges around the world.

Keywords Debris-cover effect, Ice melting, Maritime glacier, Glacier status, Mount Gongga

Citation: Zhang Y, Hirabayashi Y, Fujita K, Liu S Y, Liu Q. 2016. Heterogeneity in supraglacial debris thickness and its role in glacier mass changes of the Mount Gongga. Sci China Earth Sci, 59: 170–184, doi: 10.1007/s11430-015-5118-2

1. Introduction

Debris-covered glaciers are a prominent feature of the Tibetan Plateau and surroundings, which are characterized by the presence of supraglacial debris mantles in their ablation zones. The responses of these glaciers to climate change are considerably more complex than those of debris-free glaciers due to the debris-cover effect (Scherler et al., 2011; Benn et al., 2012). A thin debris layer accelerates ice melting relative to that of exposed snow and ice, because additional energy from the enhanced absorption of shortwave radiation resulting from the lower albedo of the debris cover transmits efficiently to the ice beneath, whereas a thicker debris layer suppresses ice melting by insulating it from atmospheric heat (Østrem, 1959; Nakawo and Young, 1981, 1982; Mattson et al., 1993; Kayastha et al., 2000). Furthermore, these glaciers generally contain a large ice volume (Paul et al., 2004; Scherler et al., 2011; Benn et al., 2012), with important consequences for the regional-scale

*Corresponding author (email: zhangy@lzb.ac.cn)

evolution of river discharge and water resources (Benn et al., 2012; Fujita and Sakai, 2014; Zhang et al., 2015). A realistic assessment of water availability and its impacts in the Tibetan Plateau and surroundings, therefore, should consider the debris-cover effect that influences mass changes by altering both rates and spatial patterns of melting. Developing a better understanding of the role of debris cover in glacier status and hydrology at a regional scale nevertheless remains a challenge, as it will require an ensemble of estimates of the extent and thickness of debris cover coupled with a large-scale mass-balance model accounting for the significance and effects of debris cover.

Difficulty of such a study arises from poor knowledge of the large-scale spatial distribution of debris thickness and properties, because field measurements of the thickness and properties of the debris layer have the practical difficulties on the large scale and methods for supraglacial debris satellite mapping remain in development (e.g., Paul et al., 2004; Suzuki et al., 2007; Mihalcea et al., 2008; Racoviteanu et al., 2009; Casey et al., 2012; Foster et al., 2012). Although recent investigations have addressed the influence of debris cover on glacier status and runoff (e.g., Lambrecht et al., 2011; Mayer et al., 2011; Scherler et al., 2011; Anderson and Mackintosh, 2012; Immerzeel et al., 2012; Lutz et al., 2014), these studies rely on simplified representations of the extent and thickness of the debris layer on the glaciers. Several numerical models have been proposed (e.g., Kayastha et al., 2000; Nicholoson and Benn 2006; Reid and Brock, 2010; Reid et al., 2012; Lejeune et al., 2013), but their applications are limited by high-quality input parameters related to the extent, thickness and thermal properties of debris cover. To remove these limitations, the methods, varying from relationships between satellite-derived surface temperature and debris thickness (e.g., Mihalcea et al., 2008; Juen et al., 2014) to the physically-based approaches (e.g., Foster et al., 2012; Rounce and McKinney, 2014), have been proposed to derive the thickness of debris cover, which can accurately estimate debris thickness from satellite imagery on their study area. Unfortunately, these methods are difficult to transfer to other glaciers or the regional scale because they require a great deal of site-specific information. Consequently, an understanding of where debris cover and its spatial distribution enhance or inhibit ice melt rates to modify its spatial characteristics and to what extent melting influences mass balance and runoff remains limited at a regional scale.

In this study, the parameter of 'thermal resistance' of the debris layer is adopted, which is defined as the debris thickness divided by the thermal conductivity of the debris layer (Nakawo and Young, 1981, 1982). Note that spatial variations of the thermal resistance can be obtained from remotely sensed data (Nakawo and Rana, 1999; Suzuki et al., 2007; Zhang et al., 2011; Fujita and Sakai, 2014), and can reflect large-scale variations in the extent and thickness of the debris layer (Zhang et al., 2011). First, we determine the spatial distribution of debris cover throughout the ablation zones of the maritime glaciers of the Mount Gongga in the south-eastern Tibetan Plateau, on the basis of the field and remote-sensing based measurements. Second, we systematically discuss the potential influences of debris cover and its spatial distribution characteristics on the average status of the Mount Gongga maritime glaciers at a regional scale and analyze the potential causes of regional differences in the debris-cover effect, using a physically-based debris-cover effect assessment model. Such work presents an integrated view of the debris-cover effect at a regional scale, which is a necessary first step toward understanding the response of debris-covered maritime glaciers to climate change and their impacts on the evolution of river discharge and water resources.

2. Study area and data

2.1 Study area

The Mount Gongga (29°20′–30°10′N, 101°30′–102°10′E; Figure 1) is located on the south-eastern margin of the Tibetan Plateau, which contains 74 maritime glaciers with an area of 257.7 km^2 and a volume of 24.65 km^3 measured from aerial photographs acquired in the 1960s (Pu, 1994). These glaciers belong to the summer-accumulation type, gaining mass mainly from summer-monsoon snowfall (Li and Su, 1996; Shi and Liu, 2000). The equilibrium-line altitudes (ELAs) vary between 4800 and 5240 m a.s.l. (Pu, 1994; Li and Su, 1996). Five glaciers, including Hailuogou (HLG) Glacier, Mozigou (MZG) Glacier, Yanzigou (YZG) Glacier, Nanmenguangou (NMGG) Glacier, and Dagongba (DGB) Glacier (Figure 1), have a length greater than 10 km and together account for 68.4% of total ice volume (Table 1). Many of these glaciers have considerable surface debris cover in their ablation zones, a consequence of the steep rocky terrain and mixed ice/snow/rock avalanche activities occurring on the surrounding walls through frost weathering processes and structural rockfalls (Li and Su, 1996). These glaciers have a high ice velocity (Song, 1994; Li and Su, 1996; Zhang et al., 2010), with maximum velocities in the order of >200 m yr^{-1} (Song, 1994; Zhang et al., 2010). Most glaciers have experienced considerable terminus retreat and mass loss since the early 20th century (Su et al., 1992; Liu et al., 2010; Zhang et al., 2010, 2012; Pan et al., 2012).

The climate of this region is characterized by the East Asian monsoon in the summer and the westerly circulation in the winter (Li and Su, 1996; Yao et al., 2012). Data from the Gongga Alpine Ecosystem Observation and Research Station (hereafter, GAEORS) located near the terminus of HLG Glacier (3000 m a.s.l.; Figure 1) show that the mean annual air temperature and precipitation are 4.1°C and ~1.9 m water equivalent (w.e.), respectively, for the period 1988–2004 (Zhang et al., 2011). Previous studies presented

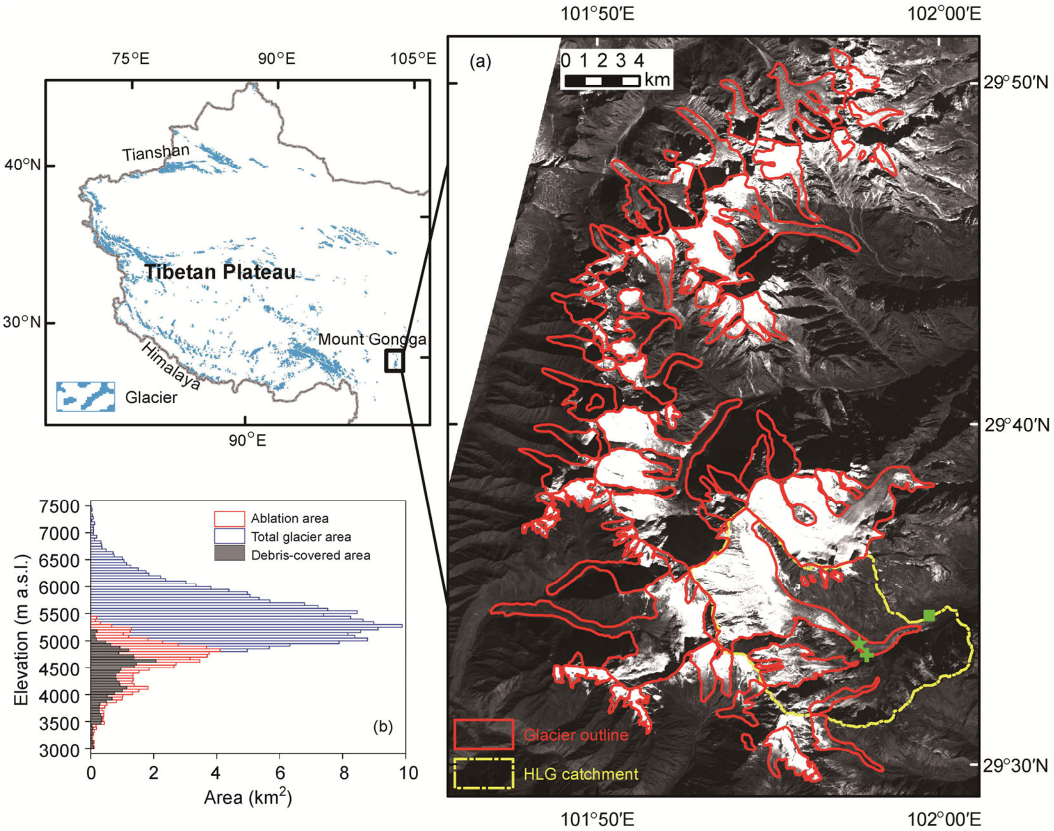

Figure 1 Map of Mount Gongga glaciers in the south-eastern Tibetan Plateau (a), and area-altitude distributions of total glacier (blue), ablation area (red) and debris-covered surface (grey) (b). The green square, star, and cross denote the Gongga Alpine Ecosystem Observation and Research Station, automatic weather station and precipitation gauge, respectively. The yellow outline is the Hailuogou (HLG) catchment.

Table 1 A summary of five debris-covered glaciers with length >10 km and their debris-cover effects[a)]

Glacier	Elevation (m a.s.l.)	Area (km^2)	Length (km)	Slope (°)	Debris coverage (%)	Debris-cover effect (%)	
						Accelerating	Insulating
HLG	2990–7556	25.7	13.1	16.0	6.4	44.0	17.0
DGB	3660–6684	21.2	11.0	7.3	16.8	3.0	56.0
MZG	3600–6886	26.8	11.6	22.2	1.74	2.0	11.0
YZG	3680–7556	32.2	11.7	13.4	11.7	41.0	50.1
NMGG	3460–6540	16.7	10.0	10.5	20.1	17.0	35.6

a) Glacier area, length, and elevation are derived from the Chinese Glacier Inventory (Pu, 1994). Mean slope is obtained from the digital elevation model. ‘Debris coverage’ denotes the debris-covered proportion of the total glacier area.

vidence for a warming trend in this region (Su et al., 1992; Liu et al., 2010; Zhang et al., 2010, 2012; Pan et al., 2012), with an increase of 0.13°C per decade between 1952 and 2009 (Zhang et al., 2012).

2.2 Data

We use various datasets, including local meteorological observations, observation-based global gridded meteorological data from the grid point closest to the glacier, four Orthorectified images of the Terra Advanced Spaceborne Thermal Emission and Reflection Radiometer (ASTER), observed debris thickness and ablation data, glacier outlines obtained in different periods, and a digital elevation model (DEM) with a resolution of 90 m. These datasets are briefly described below.

To force the detailed surface energy-mass balance model used in this study, we use a combination of local meteorological observations and observation-based global gridded data. The local meteorological observations include air temperature, precipitation, wind speed, relative humidity, and the incoming solar radiation at daily time-step observed at GAEORS (Figure 1). Daily temperature, precipitation, wind speed, and relative humidity are available for the period 1988–2007, and incoming solar radiation is available for the period 2005–2007. The observation-based global gridded datasets of daily precipitation and near-surface temperature are available for the period 1951–2007 at a spatial resolution of 0.5°. The gridded temperature dataset was generated by Hirabayashi et al. (2008) based on monthly temperature values of the Climate Research Unit version TS 2.1 dataset for the period 1951–2002 (CRU; Mitchell and Jones, 2005) and the dataset of Fan and van den Dool (2008) for the period 2003–2007. The daily precipitation dataset was created by collecting and analyzing rain-gauge observation data across Asia, the only long-term continental-scale high-resolution daily product that contains a dense network of daily rain-gauge data for Asia including the Himalayas and mountainous areas in the Middle East (Yatagai et al., 2009). The altitude information of the grid cell is derived from the 30 arc sec elevation data of the Shuttle Radar Topography Mission (http://dds.cr.usgs.gov/srtm/version2_1/SRTM30/).

The global gridded datasets of precipitation and near-surface temperature were bias-corrected on a daily timescale using linear regression equations established between the observations from GAEORS and the global gridded data over the period 1988–1997 (Zhang et al., 2012). The bias-corrected temperature and precipitation correlate well with the corresponding observations from GAEORS, yielding correlation coefficients of 0.96 and 0.87 and root mean square error (RMSE) values of 1.5°C and 0.001 m, respectively (Zhang et al., 2012). The ability of the bias-corrected global gridded data to drive the surface energy-mass balance model was verified in the HLG catchment (Figure 1), which indicates that the bias-corrected data correspond sufficiently well with the observations at GAEORS to be used as input for the model (Zhang et al., 2012). In this study, we directly use the bias-corrected gridded temperature and precipitation data.

Air temperature and precipitation data observed at an automatic weather station (AWS; 3550 m a.s.l.) and a precipitation gauge (3500 m a.s.l.) installed in the HLG catchment (Figure 1) are used for analyzing the meteorological conditions during the image acquisition days. The surface downward radiation fluxes from US National Centers for Environmental Prediction (NCEP)/US National Center for Atmospheric Research (NCAR) reanalysis 1 (Kalnay et al., 1996) are used for calculating the thermal resistance of the debris layer. These data correspond to the nearest time and location of ASTER acquisition.

To determine the spatial distribution of thermal properties of the debris cover, we use four orthorectified ASTER images, obtained on 17 December 2008 and 18 January 2009 (11:58 A.M. local time). There is no cloud or snow cover in these images. Two images were generated and distributed as Level 3A01 products by the ASTER Ground Data System (ASTER GDS) at the Earth Remote Sensing Data Analysis Center (ERSDAS) in Japan. The geography location of these images was affine-transformed by referring to a topographical map, and the RMSE of the affine transformation is within 15 m (Zhang et al., 2010). The other two images were generated and distributed by the ASTER Grid system of the Global Earth Observation Grid (GEO Grid; Sekiguchi et al., 2008). ASTER measures three visible and near infrared bands (VNIR, 0.4–0.9 μm) at a 15 m spatial resolution, six shortwave infrared bands (SWIR, 1.0–2.5 μm) at a 30 m spatial resolution, and five thermal infrared bands (TIR, 3.0–12 μm) at a 90 m spatial resolution. In this study, we use the ASTER VNIR and TIR bands.

The first *in situ* measurement of debris thickness and ablation on the Mount Gongga glaciers was carried out in 1982 at 23 sites on HLG Glacier, 19 sites on DGB Glacier, and 11 sites on Xiaogongba (XGB) Glacier (Li and Su, 1996). Systematic debris thickness measurements were made at more than 300 sites across the entire ablation zone of HLG Glacier in 2009. Ice ablation data beneath various debris thicknesses were collected on HLG, DGB, and XGB glaciers (Li and Su, 1996; Zhang et al., 2011), which are used to analyze the effect of various debris thicknesses on ice melt rates.

Glacier outlines in 1966 and 2009 are used to estimate area and terminus changes of glaciers. The glacier outline for 1966, from the Chinese Glacier Inventory (CGI; Pu, 1994), was interpreted and measured by stereophotogrammetry from aerial photographs acquired in the 1960s and corrected by aerial photographs and field investigations (Pu, 1994). The error in glacial extent estimates of the CGI varies from ±0.5% to ±1% (Pu, 1994). The glacier outline for 2009 was derived from Landsat MSS, TM, ETM+ and ASTER data using threshold ratio images, and was verified by GPS surveys on different glaciers in 2009 (Pan et al., 2012). The results of the surveys indicate that there is about ±30 m difference in the length and 0.5% error in the area (Pan et al., 2012).

ELA data of the Mount Gongga glaciers are used to determine the extents of ablation zones. Glacier ELAs recorded in the CGI (Pu, 1994) range from 4800 to 5240 m a.s.l., which were estimated from aerial photographs and topographic maps (Pu, 1994). The error in ELA estimates of the CGI is about ±50 m on average (Pu, 1994; Shi et al., 2005). The average ELA is ~4900 m a.s.l. on the eastern slope and ~5100 m a.s.l. on the western slope of the Mount Gongga (Su et al., 1992; Pu, 1994).

In addition, a DEM at a spatial resolution of 90 m was produced from aerial photographs acquired in 1989 (Zhang et al., 2010). We use it to compute the area of each elevation band and spatially distribute meteorological data.

3. Methods

3.1 Data pre-processing

We divide Mount Gongga glaciers into a set of elevation bands at intervals of 50 m based on the DEM and glacier outlines. The area of each elevation band is obtained from the DEM based on glacier outlines (Figure 1(b)). The extent of each ablation zone is determined based on the DEM and glacier outlines combined with the distribution of ELAs. In addition, the aspect of each glacier is measured from the DEM, and the mean slope of the ice surface in the ablation zones of Mount Gongga glaciers is measured along the profiles that follow the central flowline (lowermost 1–2 km, depending on glacier size).

The air temperature and precipitation time series are interpolated for each elevation band according to its mean elevation. The air temperature decreases with increasing altitude with a constant lapse rate (Table 2). The precipitation increases linearly with increasing altitude in this region (Cao and Cheng, 1994; Cheng, 1996; Liu et al., 2010). We apply a precipitation gradient (% of precipitation increase per meter of elevation increase; Table 2) from the snout to the top of the glacier, which was optimized by Zhang et al. (2012). Wind speed observed from GAEORS is not interpolated and assumed constant across the glacier surface (Zhang et al., 2012).

3.2 Debris-cover effect assessment model

To systematically and comprehensively assess the debris-cover effect on the ice-melting pattern and mass change, the debris-cover effect assessment model is proposed, which consists of two coupled components. The first is to estimate the spatial distribution of thermal resistance of the debris layer from ASTER data. The second is to compute the energy-mass change between the debris-covered/free surface and the atmosphere. This component includes three modules: a sub-debris melt module which simulates the energy available for melting from energy exchange between the debris-covered surface and the atmosphere, a debris-free melt module which calculates the energy available for melting from energy exchange between debris-free surface and the atmosphere, and an accumulation module which simulates the accumulation on the glacier and treats processes occurring in the subsurface after meltwater percolates in the underlying layers. The overall methodological framework is depicted in Figure 2.

In the model, the thermal resistance of the debris layer (R; m^2 K W^{-1}) is defined as debris thickness divided by the thermal conductivity of the debris layer (Nakawo and Young, 1981, 1982). Field surveys can obtain the thickness and thermal conductivity of the debris layer on a glacier, but field determinations of the two parameters of the debris layer are especially time-consuming and unrealistic at a large scale. The thermal resistance of the debris layer in this study is therefore calculated from the surface temperature of the debris layer derived from ASTER TIR bands and the net radiation estimated from ASTER VNIR bands and NCEP/NCAR reanalysis data, with the assumption of negligible turbulent fluxes in the energy balance (Figure 2). The approach used in this study is identical to that used in previous studies (Suzuki et al., 2007; Zhang et al., 2011). The average brightness temperature is retrieved from five TIR bands of ASTER and is used as the surface temperature on the glaciers, and the broadband albedo is estimated directly from the spectral reflectance at the top of the atmosphere in VNIR bands of ASTER. Combined with corresponding surface downward radiation fluxes from NCEP/ NCAR reanalysis data we calculate the thermal resistances of debris layers over the ablation zones of the Mount Gongga glaciers. The pixel size of ASTER TIR image is 90 m and thermal resistance is calculated using this same resolution.

According to the spatial distribution of the thermal resistance of the debris cover (Figure 3(a)), glaciers on the Mount Gongga are classified as debris-covered (R>0) and debris-free ($R\leqslant0$) surfaces. For the debris-free surface, the energy available for melting (Q_M) is calculated as:

$$Q_M = (1-\alpha)R_S + R_{Ld} + R_{Lu} + Q_S + Q_L + Q_G, \tag{1}$$

where R_S, R_{Ld} and R_{Lu} are the downward short-wave radiation flux, downward long-wave radiation flux and upward long-wave radiation flux, respectively; Q_S, Q_L and Q_G are the net sensible and latent heat fluxes and conductive heat flux into the glacier ice, respectively; and α is the surface albedo (Table 2).

For the debris-covered surface, the only heat flux considered to reach the glacier ice through the debris layer is the conductive heat flux (Q'_G) with the simplifying assumption of a linear temperature profile within the debris layer and the constant heat flux stored in the debris layer from day to day (Kraus, 1975; Nakawo and Young, 1981). The

Table 2 A summary of the value and unit of parameters used in this study

Parameter	Value	Source
Temperature lapse rate	4.3°C km^{-1}	Cao and Cheng (1994)
Precipitation gradient	18% (100 m)$^{-1}$	Zhang et al. (2012)
Snow/rain temperature threshold	2.0°C	Liu et al. (2009)
Albedo of debris-free ice	0.3	Zhang et al. (2011)
Albedo of debris-covered surface	0.2	Zhang et al. (2011)
Albedo of fresh snow	0.8	Li and Su (1996)
Density of ice	900 kg m^{-3}	Paterson (1994)
Density of snow	415 kg m^{-3}	Zhang et al. (2012)

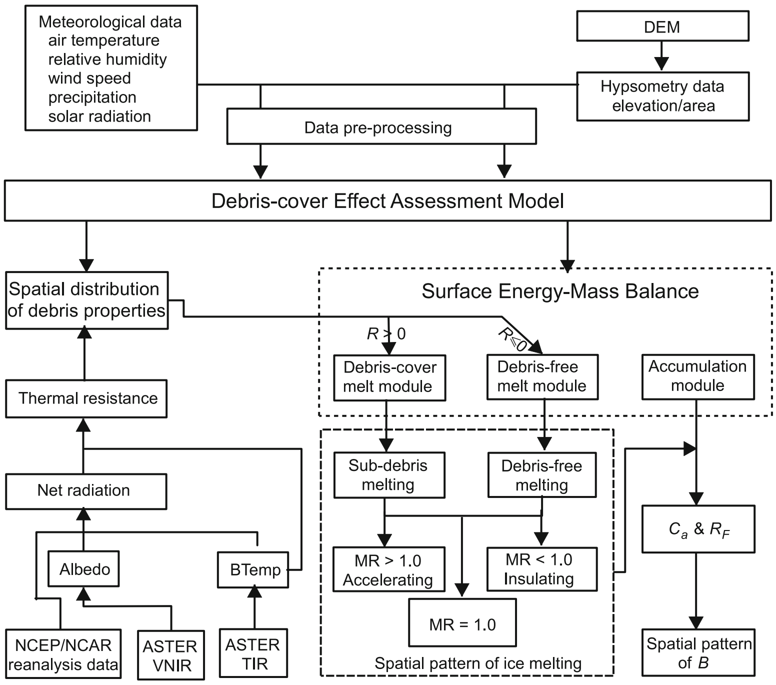

Figure 2 Overview of methodological framework. VNIP, TIR, R, C_a, R_F, MR, B, and BTemp denote visible and near infrared bands, thermal infrared bands, thermal resistance, accumulation, refreezing meltwater, melt ratio, mass balance, and brightness temperature, respectively.

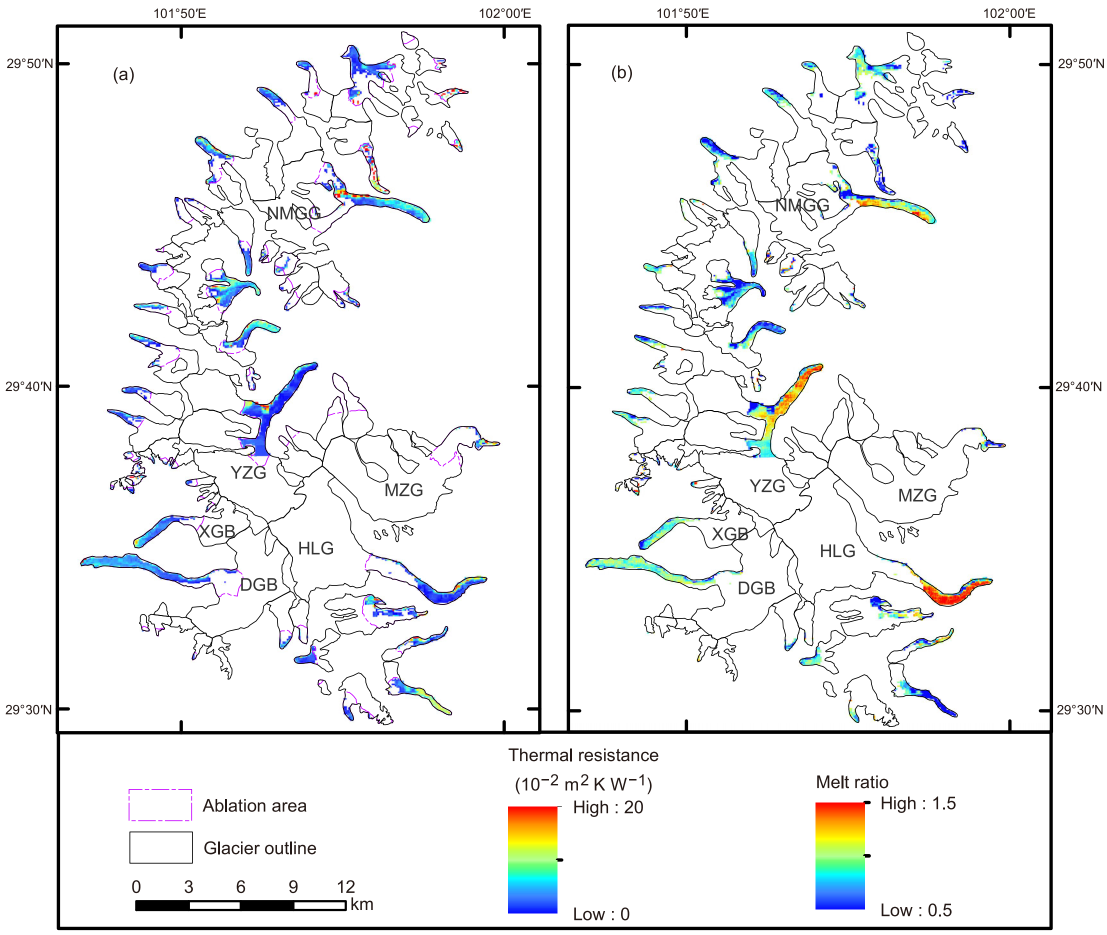

Figure 3 Spatial distributions of ASTER-derived thermal resistance of the debris layer (a) and the melt ratio (b) in the ablation zones of Mount Gongga glaciers.

energy available for melting (Q_M) is therefore calculated as:

$$\begin{cases} Q_M = Q'_G = (T_S - T_I)/R, \\ (1-\alpha')R_S + R_{Ld} + R_{Lu} + Q_S + Q_L + Q'_G = 0, \end{cases} \tag{2}$$

where α' is the albedo of debris-covered surface (Table 2), T_S is the debris surface temperature (°C), and T_I is the surface temperature of the debris-ice interface, which is assumed to be 0°C (Zhang et al., 2011).

All terms are taken to be positive toward the surface in units of W m^{-2}. The various components of the energy balance are calculated using climatic and topographic data mentioned above. Absorbed short-wave radiation is calculated from the surface albedo and downward short-wave radiation. However, downward short-wave radiation data are not available before 2005, and are estimated by applying the scheme of Zhang et al. (2012). They found a favourable correlation between precipitation and atmospheric transmissivity of solar radiation in terms of the monthly mean values. This relationship is used to estimate the daily mean transmissivity from daily precipitation data. The downward short-wave radiation is then calculated from the estimated transmissivity and the incoming shortwave radiation at the top of the atmosphere. All details of this approach are described in Zhang et al. (2012). Surface albedo, controlling the magnitude of absorption of short-wave radiation, is calculated using the method of Fujita (2007), by which the albedo is calculated using a simplified concept of multiple scattering in an ice plate having thickness related to the surface snow density (which changes with snow compaction). Upward long-wave radiation is calculated using the Stefan-Boltzmann law, and downward long-wave radiation is obtained from air temperature, relative humidity and the ratio of downward short-wave radiation to that at the top of the atmosphere using an empirical scheme (Fujita and Ageta, 2000). Relative humidity before 1988 is calculated based on the relationship between the monthly means of precipitation and relative humidity established by Zhang et al. (2012). Sensible and latent turbulent heat fluxes are obtained by bulk methods.

All energy-balance components at the glacier surface, except for the short-wave radiation term, are explicitly determined from the surface temperature. Therefore, the surface temperature for the debris-free surface is solved to satisfy all heat balance equations by iterative calculation of the conductive heat flux, which is obtained by calculating the temperature profile of the snow layer and/or glacier ice. For the debris-covered surface, the surface temperature is determined numerically by an iterative approach consistent with previous studies of debris-covered glaciers (e.g., Nicholson and Benn, 2006; Reid and Brock, 2010; Reid et al., 2012). The methods mentioned above are identical to those developed by Zhang et al. (2011, 2012), and full details are given by Zhang et al. (2011, 2012).

To assess the debris-cover effect on the ice-melting pattern, a melt ratio (MR), defined as the sub-debris melt rate (M') divided by the melt rate under the assumption of no debris in the same pixel (M), is expressed as:

$$\mathrm{MR} = M'/M, \tag{3}$$

M and M' are respectively calculated using eqs. (1) and (2) and are averaged over the period 1998–2007. A melt ratio >1.0 means that the presence of debris enhances the ice melting (hereafter termed ‘accelerating effect’ for simplicity), whereas a ratio <1.0 means that debris inhibits the ice melting (hereafter termed ‘insulating effect’ for simplicity). A melt ratio of 1.0 indicates that the ice melt rate beneath the debris layer equals that of bare ice.

No systematic direct measurement of glacier mass balance exists on the Mount Gongga, and only isolated measurements of melt rates have been made on ablation zones of DGB, XGB and HLG glaciers (Li and Su, 1996; Zhang et al., 2011). The mass balances of Mount Gongga glaciers are therefore estimated at intervals of 50 m altitude for the period 1998–2007, and computed the area-averaged mass balance using the obtained area-altitude distribution of each glacier. Therefore, the specific mass balance (B) at any location on the glacier is calculated as:

$$B = C_a + Q_M/L_f + R_F, \tag{4}$$

where C_a (positive sign) is accumulation (snow), R_F (positive sign) is refreezing, and Q_M/L_f is ablation (mass loss term is defined negatively). All terms are in units of m w.e. L_f is latent heat of fusion (Table 2). Accumulation (C_a) is modelled from the precipitation value by using a simple temperature threshold to determine whether precipitation falls as rain from snow. A mixture of snow and rain is assumed for a transition zone ranging from 1 K above and 1 K below the threshold temperature (Table 2). The refreezing amount is calculated by considering the conduction of heat into the snow layer and glacier ice and the presence of water at the interface between the snow layer and glacier ice (Fujita and Ageta, 2000). Refreezing during winter and during shorter cooling events is also considered.

Additionally, we measured changes in glacier area at the terminus from the glacier outlines of 1966 (Pu, 1994) and 2009 (Pan et al., 2012). Combined with glacier widths we calculate mean annual terminus advance or retreat rates for the period 1966–2009.

4. Results and discussion

4.1 Model performance

High-resolution *in situ* measurements of debris thickness on the Mount Gongga exist on HLG Glacier (Figure 1), which were compared to ASTER-derived thermal resistance data. This comparison indicates that ASTER-derived thermal resistances correlate reasonably well with ground-surveyed debris thicknesses over the entire ablation zone, and their spatial patterns can reflect large-scale variation in the extent and thickness of the debris cover (Zhang et al., 2011). Figure 4(a) shows along-glacier pattern of ground-surveyed debris thicknesses and ASTER-derived thermal resistances on HLG Glacier, which records continuous central flowline variation. The result indicates that along-glacier pattern of thermal resistance corresponds well with spatial pattern of ground-surveyed debris thickness. There is no high-resolution ground-surveyed debris thickness on other debris-covered glaciers of this region, and only isolated measurements exist in different altitudes on DGB and XGB glaciers (Figure 1). To assess the validity of applying thermal resistance as the proxy for debris thickness distribution on other debris-covered glaciers of this region, we compare along-glacier patterns of ground-surveyed debris thicknesses on DGB and XGB glaciers and ASTER-derived thermal resistances, which are averaged for each elevation band. Although the thermal resistance at the pixel may be affected by the ice movement, most of the thermal resistances averaged each altitude fall within standard deviations of the estimated error bounds of ground-surveyed debris thicknesses (Figures 4(b) and (c)). This implies that along-glacier patterns of thermal resistances, although the obtained periods of these data are different, are able to reflect well the spatial patterns of ground-surveyed debris thicknesses. Therefore, these results support the use of thermal resistance as the proxy for the spatial distribution of debris thickness on the Mount Gongga glaciers.

The mass balance reconstruction for the Mount Gongga glaciers was based on the ability to simulate mass balance

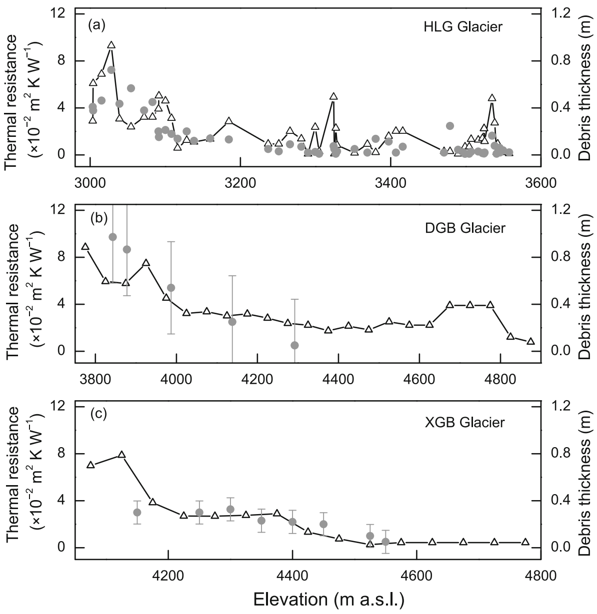

Figure 4 Comparison of ground-surveyed debris thicknesses (point) and ASTER-derived thermal resistances of debris layers (line-symbol) on HLG (a), DGB (b) and XGB (c) glaciers. Error bars denote standard deviation. See Figure 1 for glacier locations. Debris thickness data are from Li and Su (1996) and Zhang et al. (2011).

and sub-debris ice melt rates at a large scale using the surface energy-mass balance model that accounts for the debris-cover effect. The model was validated at the catchment scale through comparing the simulations to the long-term observed runoff in the HLG catchment (Zhang et al., 2012), one of the glacierized catchments of this region (Figure 1), which contains three debris-covered and four debris-free glaciers. In particular, the model considers the significance and effects of debris cover. Scatter diagram of modelled and observed ablation at stakes in different periods is shown in Figure 5(a). Overall, the model performs well at stake locations observed in different periods with the RMSE value of 0.003 m w.e. d^{-1} compared to the mean melt rate of 0.03 m w.e. d^{-1}. A comparison of modelled and observed melt rates at different thicknesses of the debris layer (Figure 5(b)) reveals that simulations at different debris thicknesses are in good agreement with observed melt rates. These results confirm that the model can produce reliable estimates of ice melt rates beneath various debris thicknesses. According to the calculation, the mean annual mass balance in the whole region is –0.63 m w.e. over the period 1998–2007, which is similar to the mass loss rate (–0.4±0.41 m w.e.) in this region over the period 2003–2009 estimated by Gardner et al. (2013). In addition, the overall aim of this study is not to simulate as accurately as possible the mass balance or spatial variations for any given year but rather to systematically evaluate the impacts of the spatial distribution of debris cover on the average status of Mount Gongga glaciers. In this respect, the model is able to simulate the mass balance for the Mount Gongga glaciers which is in a plausible and realistic range.

4.2 Thermal resistance of the debris cover

Figure 3(a) shows the spatial distribution of ASTER-derived thermal resistance of the debris layer over the ablation zones of the Mount Gongga glaciers. Relatively high values of thermal resistance are generally found at the termini of glaciers and lower values occur mainly in the upper reaches of the ablation zones. Such a trend corresponds well with the observed spatial pattern of debris cover in the field, i.e., the debris cover is thick and continuous at the termini and is thin and patchy in the upper reaches of the ablation zones. Spatial patterns of ground-surveyed debris thicknesses (Figure 4) and thermal resistances of debris layers (Figure 3(a)) on different glaciers all reveal the same variation trend of debris thickness, a downglacier increase, but considerably spatial variability exists at each site. Systematic debris thickness measurements in this region have been made only on HLG Glacier. These measurements indicate that debris emerges on the glacier surface below the icefall at ~3600 m a.s.l., from which its thickness increases to more than 1.0 m near the terminus. According to *in situ* surveys of debris thickness on HLG Glacier (Figure 4(a)), we found that the debris cover is thick in the altitude range of

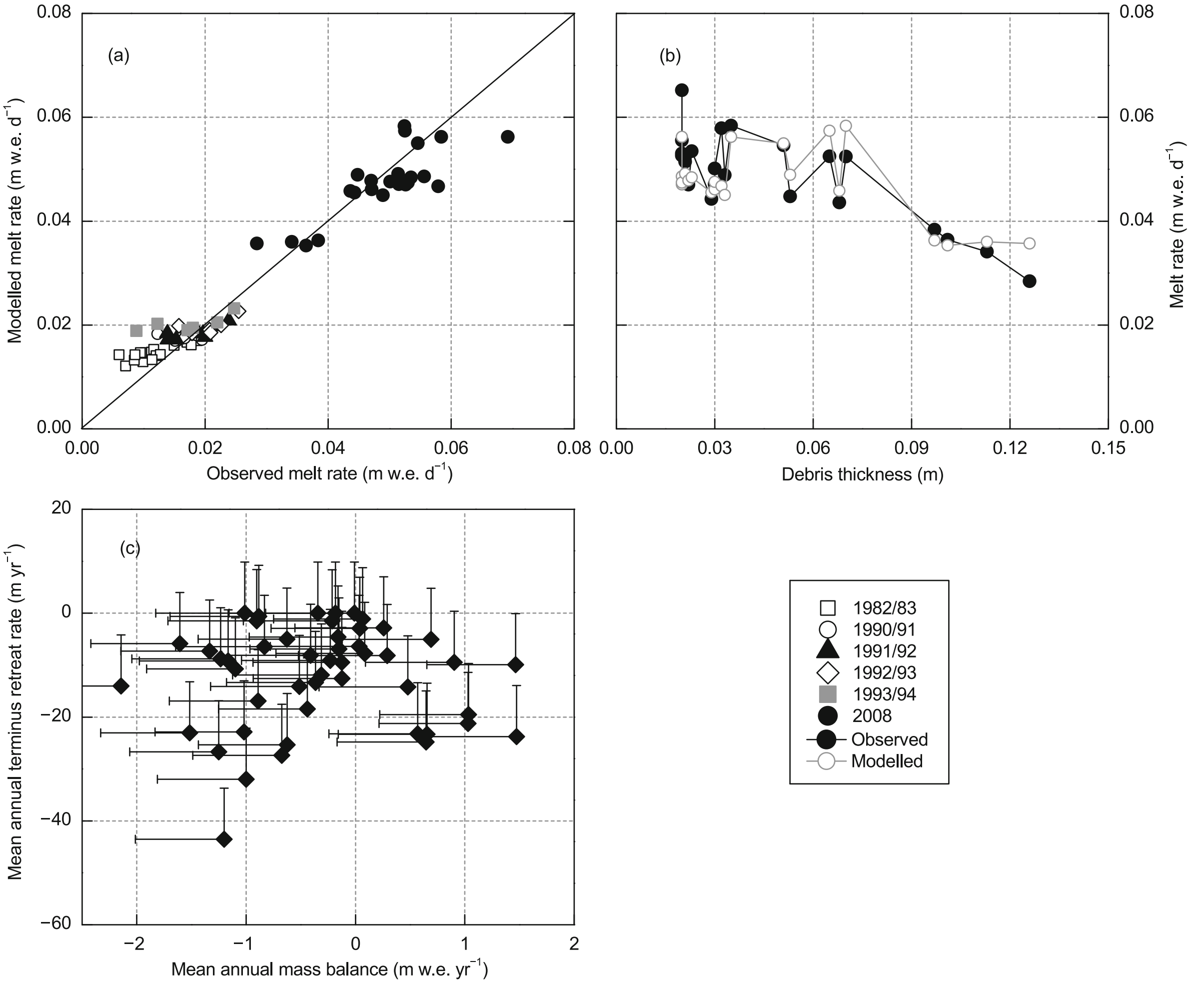

Figure 5 Comparisons of observed and modelled ice melt rate in different periods (a) and at various debris thicknesses (b), and mean annual mass balances and mean annual terminus retreat rates (c). Error bars indicate the standard deviation. Melt rate data are derived from Zhang et al. (2011, 2012).

2900–3100 m a.s.l., where its mean thickness is ~0.4 m, and the debris cover is thin in the altitude range of 3100–3600 m a.s.l., where its mean thickness is ~0.09 m. Of the *in situ* debris thickness measurements, ~50.3% have a debris thickness of less than 0.1 m and ~25% have a thickness of less than 0.03 m. Debris thicknesses and ASTER-derived thermal resistances along transverse profiles, which were constructed across representative areas of HLG Glacier (terminus, central and upper parts of the ablation zone) (Zhang et al., 2011), indicate the considerably inhomogeneous distribution in space, especially at the profiles near the terminus where the debris thickness varies from a few centimeters to more than 1.0 m.

Field observation on the Himalayan glacier revealed a critical thickness of 0.03 m (Mattson et al., 1993), at which sub-debris melt rate equals clean-ice or -snow melt rate (Adhikary et al., 1997). However, there is no such an experiment on the Mount Gongga glaciers. Hence, we calculate the thermal resistance for 0.03 m debris layer on the basis of the relationship between the debris thickness and thermal resistance. This relationship is established using more than 300 ground-surveyed debris thicknesses and corresponding ASTER-derived thermal resistances on HLG Glacier (Zhang et al., 2011). The calculated thermal resistance for 0.03-m debris layer is about 1.35×10^{-2} m^2 K W^{-1}. We found that ~27% of the total debris-covered area on Mount Gongga glaciers has a thermal resistance value smaller than it. As noted above, debris thickness revealed by the spatial distribution of ASTER-derived thermal resistances of debris layers (Figure 3(a)) shows a significant inhomogeneous spatial distribution; in particular, the thin debris cover <0.03 m is widely distributed on Mount Gongga glaciers.

We class these glaciers as debris-covered and debris-free glaciers on the basis of the spatial distribution of the thermal resistance of the debris layer (Figure 3(a)). Among 74 glaciers on the Mount Gongga, 50 glaciers are covered with a varying thickness of debris. These glaciers represent 68.0% and 93.4% of the total glacier number and area of region. The proportion of debris cover to the total glacier area varies from 1.74% to 53.0%. The total debris-covered area is ~32 km^2, accounting for as much as 13.5% of the total glacier area of the region (Figure 1(b)). Debris covers most of the ablation zone below 3800 m a.s.l. (Figure 1(b)), but the area of debris-covered surface across the elevation band between 3800 and 4800 m a.s.l. represents 82% of the total debris-covered area, and only 7% of the debris cover occurs above 4800 m a.s.l. In particular, debris cover occurs predominantly in the tongues of large valley glaciers, and the volume of debris-covered glaciers with an area >5 km^2 accounts for as much as 78.3% of the total glacier volume of the Mount Gongga. Among the five glaciers with length >10 km in the region (Table 1), NMGG Glacier (Figure 1) has the largest debris cover, ~20.1% of the total glacier area, and HLG Glacier, the longest glacier on the Mount Gongga, has ~6.4% debris cover.

4.3 Debris-cover effects on Mount Gongga glaciers

Figure 3(b) shows the spatial distribution of the melt ratio on Mount Gongga glaciers. About 10.2% of the total ablation area of debris-covered glaciers, where the melt ratio is >1.0, has experienced accelerated melting, ~40.8% of the total ablation area, where the melt ratio is <1.0, has undergone inhibited melting, and ~49% of the total ablation area has the melt ratio equal to 1.0 (Figure 3(b)). Five glaciers of the region have lengths >10 km and all of these have debris cover (Figure 3). Their debris-covered proportions of total glacier area vary from 1.74% to 20.1% (Table 1). Only one of the five glaciers, HLG Glacier, is characterized by significant accelerating effect of debris cover. About 44% of the ablation zone on HLG Glacier experiences accelerated melting, and ~17% of the ablation zone experiences inhibited melting (Table 1). YZG Glacier, the largest glacier in the region, has 11.7% debris cover (Table 1), where accelerating and insulating effects of debris cover in the ablation zone are almost the same. The remaining three glaciers show significant insulating effect of debris cover in their ablation zones (Table 1).

In situ ablation measurements beneath various debris thicknesses on HLG, XGB, and DGB glaciers indicate that debris thickness principally controls sub-debris melt rates and its small change results in a marked change in the ice melt rate. The mean debris thickness on DGB Glacier (~0.54 m) is significantly larger than that on HLG Glacier (~0.16 m) (Figure 4), a difference also revealed by the spatial distribution of thermal resistance (Figure 3(a)), with the consequence that the two glaciers show opposite trends in the debris-cover effect (Table 1). As shown in Figure 3a, debris-covered glaciers on the Mount Gongga have an apparently inhomogeneous distribution of debris thickness and widespread thin debris cover. Consequently, spatial differences in the debris-cover effect on the ice-melting pattern are apparent on these glaciers (Figure 3(b)), making it completely different from the up-glacier decrease in the ablation gradient on debris-free glaciers. Such altered spatial patterns of melting will lead to significant spatial variability in the regional ablation regime.

Model results reveal a mean annual mass loss rate of –0.63 m w.e. yr^{-1} for the whole of Mount Gongga glaciers for the period 1998–2007, suggesting negative balance conditions for the region. To comprehensively assess the impact of debris cover on the mass loss of the whole region, we recalculated the mean annual mass balance under the assumption of no debris cover on the debris-covered glaciers. A comparison of the mass balances under the plausibly real surface condition with those of the no-debris assumption indicates that mass loss is accelerated on ~25% of the debris-covered glaciers where the debris-covered proportion is less than 20% and that mass loss is inhibited with increasing debris-covered proportion relative to the no-debris-assumption case (Figure 6). Although glaciers with debris-covered proportions >20% experience inhibited mass loss compared to that of the no-debris assumption, regionally averaged mass loss of debris-covered glaciers is similar to that of debris-free glaciers, which is contrary to expectations.

4.4 Regional differences in the debris-cover effect

The significant effect of debris cover in other regions is to reduce mass loss from the glacier, although differences in the proportion of debris cover are apparent from region to region (Table 3). *In situ* measurements of debris thickness indicate that debris thickness on debris-covered glaciers of other regions (Table 3) is generally thicker than that on Mount Gongga glaciers. Previous investigations have addressed the impact of debris cover on glacier status and runoff at a large scale, but they only accounted for the effect of thick debris cover using a multiplicative reduction factor (e.g., Anderson and Mackintosh, 2012; Immerzeel et al.,

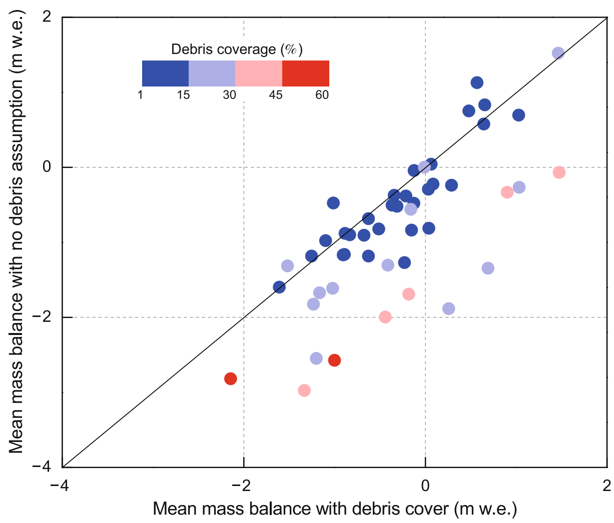

Figure 6 Comparison of mean mass balance of debris-covered glaciers calculated with the real surface condition and that calculated with the no-debris assumption. Marker-symbol colors denote the debris-covered proportion of total glacier area.

Table 3 Regional differences in the debris-cover effect. MRF is multiplicative reduction factor

Region	Debris (%)	Debris-cover effect	Debris thickness	Reference
South Alps, New Zealand	8.0	Insulating effect	0–3 m Consider thick debris with a MRF	Anderson and Mackintosh (2012)
Caucasus	8.1–23.0	Insulating effect	Extrapolation from observed thicknesses on few glaciers[b)]	Lambrecht et al. (2011)
Altay	3.7–25.8	Insulating effect	Extrapolation from observed thicknesses on few glaciers[b)]	Mayer et al. (2011)
Tuomur, Tien Shan	7.5–22.0	Insulating effect, and accelerating in 2%[a)] of ablation area	0–2.5 m Some large rocks piled up to several meters	Su et al. (1985) Zhang et al. (2006) Zhang et al. (2007)
Himalaya & Karakorum	2.0–36.0	Insulating effect	Consider the extent of debris	Scherler et al. (2011)
Langtang, Himalaya	19.0	Insulating effect	Use a MRF (0.15/0.7)	Immerzeel et al. (2012)
Mount Gongga	13.5	Accelerating effect in 10.2% of ablation area, and insulating in 40.8 %	0–1.4 m Consider spatial distribution of debris thickness	This work

a) It is calculated from observed data of Su et al. (1985). b) Regional debris thicknesses are extrapolated from observed thicknesses on a few glaciers with an assumption of similar thickness/elevation distribution on the neighbouring glaciers.

2012) or regional debris thickness extrapolated from the thickness measurements on a few glaciers with an assumption of similar thickness/elevation distributions on the neighbouring glaciers (e.g., Lambrecht et al., 2011; Mayer et al., 2011) (Table 3). In contrast, our investigation comprehensively considered debris thickness and its spatial characteristics revealed by the ASTER-derived thermal resistance of the debris layer on the glaciers, with the consequence that we found apparently spatial differences in the debris-cover effect on the average status of the Mount Gongga maritime glaciers. In particular, the presence of debris and its inhomogeneous distribution accelerate the melting on ~10.2% of the total ablation zone and produce a more negative mass balance on ~25% of the debris-covered glaciers. Furthermore, a widely distributed surface on the Mount Gongga glaciers, composed of co-existing debris-covered ice, bare ice, ice cliffs and supraglacial ponds in the ablation zone, makes disproportionately large contributions to ablation (Sakai et al., 2000, 2002). Consequently, regionally averaged mass loss of debris-covered glaciers is similar to that of debris-free glaciers on the Mount Gongga, which is contrary to expectations. This phenomenon was also found on Himalaya glaciers (Kääb et al., 2012), where regionally averaged thinning rates on debris-covered ice are similar to those of debris-free ice despite the widely assumed insulating effect of debris cover.

In addition, we observed that the termini of debris-covered glaciers show significant retreat with some of the highest retreat rates compared to those of debris-free glaciers. Between 1966 and 2009, both retreating and stable glacier termini existed with rates between –45.0 and 0 m yr^{-1} (Figure 7), and 90% of the glaciers were retreating. The mean retreat rate for the whole of Mount Gongga glaciers is about 10.0 m yr^{-1} for the period 1966–2009, above which is defined as significant retreat. About 29% of the debris-free glaciers showed significant retreat, whereas 51% of debris-covered glaciers showed significant retreat with some of the highest retreat rates (~ –45 m yr^{-1}) on the Mount Gongga. We observed that debris-free glaciers with mean slopes >30° exhibited larger retreat rates, and those with mean slopes <20° had smaller retreat rates (Figure 7). In contrast, debris-covered glaciers with gentle slopes exhibited larger retreat rates when the debris-covered proportion is relatively large, and those with steep slopes had relatively smaller retreat rates when the debris-covered proportion is relatively small (Figure 7). Our finding is different from many eastern and central Himalayan debris-covered glaciers with stagnant low-gradient terminus regions (Scherler et al., 2011).

According to *in situ* observations of ice velocities on

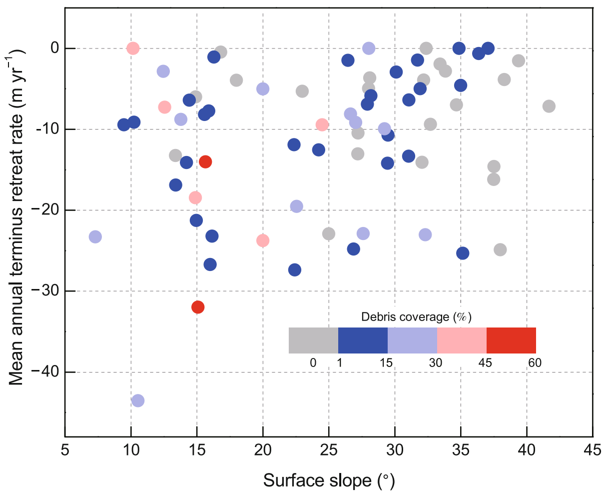

Figure 7 Scatter plot of mean annual terminus retreat rates versus mean surface slopes of the ablation zones of debris-covered and debris-free (grey dots) glaciers. Marker-symbol colors denote the debris-covered proportion of total glacier area.

HLG, DGB and XGB glaciers during different periods (Song, 1994; Li and Su, 1996; Zhang et al., 2011), the ice velocities of these glaciers are largely higher than those of glaciers in other regions of the Tibetan Plateau (Li and Su, 1996; Shi and Liu, 2000). Ice velocities in the ablation zone of HLG Glacier generally vary from 28.8 to 205.0 m yr^{-1} (Zhang et al., 2010). In contrast, most Himalaya glaciers have low ice velocities and shallow termini (Scherler et al., 2011; Benn et al., 2012). Note that mean surface slopes in the terminus region of <8° promote the development of stagnant ice (Scherler et al., 2011). Mean surface slopes in the terminus regions of most debris-covered glaciers on the Mount Gongga are greater than 8°, which facilitate frequent rock falls and snow avalanches (Li and Su, 1996). It must be pointed out that the widespread presence of supraglacial debris and ponds on these glaciers can accelerate glacier terminus disintegration by exposing ice faces at the surface (Röhl, 2008), lowering the glacier surface (Sakai and Fujita, 2010) and backwasting, a related topographic inversion processes, can yield complex debris assemblages and numerous supraglacial ponds (Benn and Evans, 2010, Benn et al., 2012). Consequently, high ice velocities, relatively steep surface slopes and the intensely inhomogeneous ice melting caused by widespread debris cover lead to the unstable fronts of the debris-covered glaciers on the Mount Gongga, which accelerates their terminus disintegration and retreat.

4.5 Uncertainties in estimations of thermal resistances and mass balance

The main sources of uncertainty in calculating the thermal resistance of the debris layer using ASTER images come from neglecting the turbulent heat fluxes in the surface energy-balance calculation, the shading effect by surrounding mountains and the presence of water. The approach used in this study is based on the fact that the net radiation is usually the dominant heat source on debris-covered glaciers in the Tibetan Plateau and the contribution of the turbulent heat fluxes to the total energy balance is normally small (e.g., Mattson and Gardner, 1991; Kayastha et al., 2000; Takeuchi et al., 2000; Suzuki et al., 2007), which can be neglected. Zhang et al. (2011) found the same characteristic of the energy balance at the debris-covered surface on HLG Glacier of this region, especially at the debris layer of >0.1 m. On the other hand, several studies suggested that with the exception of the net radiation, the turbulent heat fluxes play an important role in the debris surface energy balance (e.g. Brock et al., 2010; Reid et al., 2012; Lejeune et al., 2013). Therefore, to evaluate the uncertainty in the approach caused by neglecting the turbulent heat fluxes in the surface energy-balance calculation, thermal resistances of debris layers were calculated from observed meteorological data using two methods: One considers all components of the debris surface energy balance, and the other only considers the net radiation (Suzuki et al., 2007). The results confirm that this assumption is unlikely to affect the spatial pattern of the thermal resistance of the debris layer.

Although the shading of solar insolation by surrounding mountains may not affect the thermal resistance of the debris layer (Suzuki et al., 2007), the presence of water in the debris does (Nicholson and Benn, 2006; Suzuki et al., 2007; Zhang et al., 2012). Hence, knowledge of the meteorological conditions at, before and after the image acquisition date is of vital importance for calculating thermal resistance from ASTER data. Image acquisition in this study is near the middle of the dry winter season of this region, where 75%–90% of the annual precipitation falls in the months of May–October and the mean annual air temperature is high (Su et al., 1992; Li and Su, 1996; Zhang et al., 2010). According to the observations at AWS and at the precipitation gauge (Figure 1), we analyzed the meteorological conditions at the time of ASTER acquisition, and found that the air temperatures are 1.8 and 5.7°C on 17 December 2008 and 18 January 2009, respectively, with low relative humidity (<30%), low wind speed (<0.75 m s^{-1}), almost no clouds and no precipitation. Furthermore, the meteorological conditions before and after the image acquisition date are analyzed based on the meteorological observations, which are characterized by high temperatures, cloud-free skies, and prolonged lack of precipitation. The debris surface is therefore considered to be dry in the calculation of thermal resistance.

The surface downward radiation fluxes from NCEP/NCAR reanalysis 1 that correspond to the nearest time and location of ASTER acquisition can cause the uncertainty for the calculation of the thermal resistance of the debris layer. Earlier investigations, which estimated the thermal resistance on different glaciers using the same approach and dataset (Suzuki et al., 2007; Zhang et al., 2011), indicated that the spatial patterns of estimated thermal resistances of debris layers correspond well with the spatial patterns of debris thickness, reflecting large-scale variations in the extent and thickness of the debris cover. Meanwhile, the estimated thermal resistances correlated reasonably well with ground-surveyed debris thicknesses (Zhang et al., 2011). We calculated the thermal resistance of the debris layer in thickness of 0.1 m on the basis of the relationship between ground-surveyed debris thicknesses and ASTER-derived thermal resistances (Zhang et al., 2011). The thermal resistance for the debris layer in thickness of 0.1 m is about 0.0192 m^2 K W^{-1}, and its thermal conductivity (the ratio of debris thickness and thermal resistance) is about 5.19 W^{-1} m K^{-1}. These results are in the similar order with those of Lambrecht et al. (2011), who calculated the thermal resistance in a 0.1 m thick layer for different rock types and thermal conductivity of the respective material.

As discussed above, we believe that the estimated thermal resistance can present a reasonable view of the spatial distribution of debris thickness on Mount Gongga glaciers. It possibly provides important insight into studying debris-covered glaciers without *in situ* measurements of the extent, thickness, and thermal properties of the debris layer at a large scale.

Additionally, glacier mass balance estimation is based on the ability of a surface energy-mass balance model with debris treatment to simulate mass balance and sub-debris ice melt rate at a large scale. The model was validated at the catchment scale by comparing the simulations to observed runoff and glacier ablation for different periods in the HLG catchment (Zhang et al., 2012). In the calculation, an assumption was made of model parameters that are constant in both space and time (Table 2). Thermal resistances of debris layers were also considered as constant in the ablation zones of the glaciers, although the thermal resistance at a specific pixel may be affected by the ice movement and deposition of supraglacial debris due to the high ice velocity of Mount Gongga glaciers (Song, 1994; Li and Su, 1996; Zhang et al., 2010). Comparison of ASTER-derived thermal resistances in 2008 with those in 2009 at the same pixels on Mount Gongga glaciers indicates that little difference exists in thermal resistances derived from the independent data (Figure 8). The overall correlation coefficient between thermal resistances in 2008 and those in 2009 is 0.72 (significance level $P<0.001$). This finding is in agreement with previous studies (Rana et al., 1997; Nakawo and Rana, 1999; Suzuki et al., 2007), which suggested that the thermal resistance of the debris layer can usually be regarded as constant on debris-covered glaciers. Despite this uncertainty, the model results for the HLG catchment confirmed that the model reconstructed well the long-term mass balance (1952–2009) (Zhang et al., 2012). In particular, the model was able to reliably estimate the ice melt rates beneath various debris thicknesses during different periods (Figures 5(a) and (b)). The mean annual mass balances of the Mount Gongga glaciers are calculated for the period 1966–2007

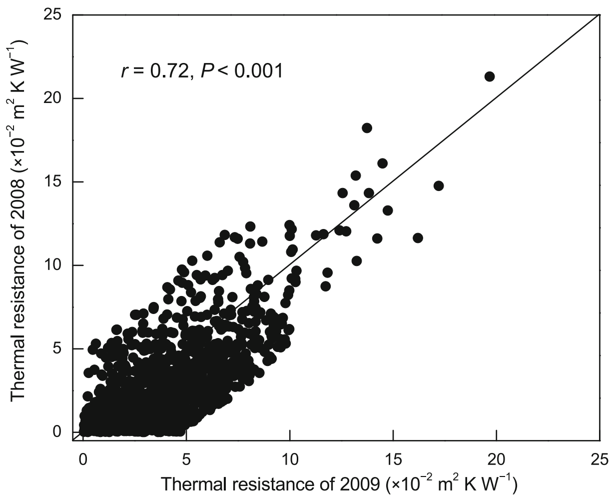

Figure 8 Comparison of the 2008 and 2009 ASTER-derived thermal resistances at the same pixels on Mount Gongga glaciers. The letters r and P denote the correlation coefficient and significance level, respectively.

using a combination of local meteorological observations and observation-based global gridded data, which are compared to their mean annual terminus retreat rates over the period 1966–2009. The result indicates that the mass balance calculated by the surface energy-mass balance model can capture the trend of rapid retreat of the glaciers (Figure 5(c)). As noted above, we believe that the model presents a reasonable view of the general condition of the mass balance of Mount Gongga glaciers, which possibly provides a useful context for discussing the potential impacts of debris cover and its spatial distribution on the average status of debris-covered glaciers at a large scale.

5. Conclusions and outlook

The Mount Gongga offers an opportunity to study a monsoonal maritime glacier system with debris-covered and debris-free glaciers in the south-eastern Tibetan Plateau, where specific, though incomplete, information is available for both the glaciology and meteorology. Sixty-eight percent of Mount Gongga glaciers have extensive mantles of supraglacial debris in the ablation zones, where the debris-covered proportions of the total glacier area vary from 1.74% to 53.0%. These glaciers show a general downglacier increasing trend in debris thickness with significant spatial inhomogeneity at each site. Spatial distribution of debris thickness revealed by the ASTER-derived thermal resistance indicate that thin debris thicknesses of <0.03 m are widely distributed on the glaciers.

Against the background of global warming, the presence of supraglacial debris has a significant insulating effect on the trend of greater negative mass balance on the debris-covered glaciers, especially on the glaciers with debris-covered proportions >20%. But it accelerates the trend of faster ice melting on ~10.2% of the total ablation area and produces a more negative mass balance, which is caused primarily by temperature rise, on ~25% of the debris-covered glaciers on the Mount Gongga. The consequence is that regionally averaged mass balance of debris-covered glaciers is not statistically different from that of debris-free glaciers with all glaciers exhibiting an intensive negative mass balance trend on the Mount Gongga. Also, the intensely inhomogeneous ice melting caused by widespread debris cover in association with high ice velocities and relatively steep surface leads to active terminus regions of the debris-covered glaciers, of which the termini showed significant retreat compared to those of the debris-free glaciers.

Debris-covered glaciers are common on the Tibetan Plateau and surroundings, as well as in many other mountain ranges around the world (Nicholson and Benn, 2006; Brock et al., 2010; Anderson and Mackintosh, 2012; Brenning et al., 2012; Reid et al., 2012). Although the percentages of debris cover of the studied debris-covered glaciers vary from 2% to 36% (Table 3), the impact of the debris cover on both the ice-melting rates and spatial patterns of mass loss is significant in each region. In particular, it shows apparent systematic differences from region to region, with the consequence that the inclusion of debris cover in estimates of glacier mass balance and runoff at a large scale is of vital importance. Despite numerous simplifications, our physically-based techniques for mapping the distribution of supraglacial debris thickness using satellite imagery and estimating the effects of debris cover can systematically assess the significance of debris cover and its influence on spatial patterns of ice melting and mass balance at a regional scale. These approaches possibly provide an important insight into studying the average status of debris-covered glaciers and its impacts at the regional scale, including long-term variation of mass balance and water resources and increased frequency of glacier lake outburst floods.

Acknowledgements *We thank the Gongga Alpine Ecosystem Observation and Research Station (GAEORS) of the Chinese Ecological Research Network and the AIST GEO for providing the meteorological data and ASTER data, respectively. We thank Dr. PAN Baotian of Lanzhou University for providing 2009 glacier outline data for the Mount Gongga. We thank the anonymous reviewers for their valuable comments and suggestions. This work was supported by the National Science and Technology Support Program of China (Grant No. 2012BAC19B07), the National Natural Science Foundation of China (Grant No. 41190084), the Ministry of Science and Technology of China (MOST) (Grant No. 2013FY111400), and CREST Project of Japan Science and Technology Agency.*

References

Adhikary S, Seko K, Nakawo M, Ageta Y, Miyazaki N. 1997. Effect of surface dust on snow melt. Bull Glaciol Res, 15: 85–92

Anderson B, Mackintosh A. 2012. Controls on mass balance sensitivity of maritime glaciers in the Southern Alps, New Zealand: The role of debris cover. J Geophys Res, 117: F01003

Benn D I, Evans D J. 2010. Glaciers and Glaciation. London: Hodder Education

Benn D I, Bolch T, Hands K, Gulley J, Luckman A, Nicholson L I, Quincey D, Thompson S, Toumi R, Wiseman S. 2012. Response of debris-covered glaciers in the Mount Everest region to recent warming, and implications for outburst flood hazards. Earth-Sci Rev, 114: 156–174

Brenning A, Peña M A, Long S, Soliman, A. 2012. Thermal remote sensing of ice-debris landforms using ASTER: An example from the Chilean Andes. Cryosphere, 6: 367–382

Brock B W, Mihalcea C, Kirkbride M P, Diolaiuti G, Cutler M E J, Smiraglia C. 2010. Meteorology and surface energy fluxes in the 2005–2007 ablation seasons at the Miage debris-covered glacier, Mont Blanc Massif, Italian Alps. J Geophys Res, 115: D09106

Cao Z, Cheng G. 1994. Preliminary analyses of hydrological characteritics of Hailuogou Glacier on the eastern slope of the Gongga Mountain. In: Xie Z, Kotlyakov V M, eds. Glaciers and Environment in the Qinhai-Xizang (Tibet) Plateau (I)—The Gongga Mountain. Beijing and New York: Science Press. 143–156

Casey K A, Kääb A, Benn D I. 2012. Geochemical characterization of glacier debris cover via *in situ* and optical remote sensing methods: A case study in the Khumbu Himalaya, Nepal. Cryosphere, 6: 85–100

Cheng G. 1996. Exploration of precipitation features on extra-high zone of Mt Gongga (in Chinese). Mt Res, 14: 177–182

Fan Y, van den Dool H V D. 2008. A global monthly land surface air temperature analysis for 1948–present. J Geophys Res, 113: D01103

Foster L A, Brock B W, Cutler M E J, Diotri F. 2012. A physically based method for estimating supraglacial debris thickness from thermal band remote-sensing data. J Glaciol, 58: 677–691

Fujita K, Ageta Y. 2000. Effect of summer accumulation on glacier mass balance on the Tibetan Plateau revealed by mass-balance model. J Glaciol, 46: 244–252

Fujita K. 2007. Effect of dust event timing on glacier runoff: Sensitivity analysis for a Tibetan glacier. Hydrol Process, 21: 2892–2896

Fujita K, Sakai A. 2014. Modelling runoff from a Himalayan debris-covered glacier. Hydrol Earth Syst Sci, 18: 2679–2694

Gardner A S, Moholdt G, Cogley J G, Wouters B, Arendt A A, Wahr J, Berthier E, Hock R, Pfeffer W T, Kaser G, Ligtenberg S R M, Bolch T, Sharp M J, Hagen J O, van den Broeke M R, Paul F. 2013. A reconciled estimate of glacier contributions to sea level rise: 2003 to 2009. Science, 340: 852–857

Hirabayashi Y, Kanae S, Emori S, Oki T, Kimoto, M. 2008. Global projections of changing risks of floods and droughts in a changing climate. Hydrol Sci J, 53: 754–772

Immerzeel W, van Beek L P H, Konz M, Shrestha A B, Bierkens M F P. 2012. Hydrological response to climate change in a glacierized catchment in the Himalayas. Clim Change, 110: 721–736

Juen M, Mayer C, Lambrecht A, Han H, Liu S. 2014. Impact of varying debris cover thickness on ablation: A case study for Koxkar Glacier in the Tien Shan. Cryosphere, 8: 377–386

Kääb A, Berthier E, Nuth C, Gardelle J, Arnaud Y. 2012. Contrasting patterns of early twenty-first-century glacier mass change in the Himalayas. Nature, 488: 495–498

Kalnay E, Kanamitsu M, Kistler R, Collins W, Deaven D, Gandin L, Iredell M, Saha S, White G, Woollen J, Zhu Y, Chelliah M, Ebisuzaki W, Higgins W, Janowiak J, Mo KC, Ropelewski C, Wang J, Leetmaa A, Reynolds R, Jenne R, Joseph D. 1996. The NCEP/NCAR 40-year reanalysis project. Bull Amer Meteorol Soc, 77: 437–471

Kayastha R B, Takeuchi Y, Nakawo M, Ageta Y. 2000. Practical prediction of ice melting beneath various thickness of debris cover on Khumbu Glacier, Nepal, using a positive degree-day factor. Int Assoc Hydrol Sci Publ, 264: 71–81

Kraus H. 1975. An energy balance model for ablation in mountainous areas. Int Assoc Hydrol Sci Publ, 104: 74–82

Lambrecht A, Mayer C, Hagg W, Popovnin V, Rezepkin A, Lomidze N, Svanadze D. 2011. A comparison of glacier melt on debris-covered glaciers in the northern and southern Caucasus. Cryosphere, 5: 525–538

Lejeune Y, Bertrand J-M, Wagnon P, Morin S. 2013. A physically based model of the year-round surface energy and mass balance of debris-covered glaciers. J Glaciol, 59: 327–344

Li J, Su Z. 1996. Glaciers in the Hengduan Mountains (in Chinese). Beijing: Science Press. 1–110

Liu Q, Liu S, Zhang Y, Wang X, Zhang Y, Guo W, Xu, J. 2010. Recent shrinkage and hydrological response of Hailuogou glacier, a monsoon temperate glacier on the east slope of Mount Gongga, China. J Glaciol, 56: 215–224

Liu S, Zhang Y, Zhang Y S, Ding Y. 2009. Estimation of glacier runoff and future trends in the Yangtze River source region, China. J Glaciol, 55: 353–362

Lutz A F, Immerzeel W W, Shrestha A B, Bierkens M F P. 2014. Consistent increase in High Asia's runoff due to increasing glacier melt and precipitation. Nature Clim Change, 4: 587–592

Mattson L E, Gardner J S, Young G J. 1993. Ablation on debris covered glaciers: An example from the Rakhiot Glacier, Punjab, Himalaya. Int Assoc Hydrol Sci Publ, 218: 289–296

Mattson L E, Gardner J S. 1991. Energy exchanges and ablation rates on the debris-covered Rakhiot Glacier, Pakistan. Z Gletscherk Glazialgeol, 25: 17–32

Mayer C, Lambrecht A, Hagg W, Narozhny Y. 2011. Glacial debris cover and melt water production for glaciers in the Altay, Russia. Cryosphere Discuss, 5: 401–430

Mihalcea C, Brock B W, Diolaiuti G, D'Agata C, Citterio M, Kirkbride M P, Cutler M E J, Smiraglia C. 2008. Using ASTER satellite and ground-based surface temperature measurements to derive supraglacial debris cover and thickness patterns on Miage Glacier. Cold Reg Sci Technol, 52: 341–354

Mitchell T D, Jones P D. 2005. An improved method of constructing a database of monthly climate observations and associated high-resolution grids. Int J Climatol, 25: 693–712

Nakawo M, Rana B. 1999. Estimate of ablation rate of glacier ice under a supraglacial debris layer. Geogr Ann, 81A: 695–701

Nakawo M, Young G J. 1982. Estimate of glacier ablation under a debris layer from surface temperature and meteorological variables. J Glaciol, 28: 29–34

Nakawo M, Young G J. 1981. Field experiments to determine the effect of a debris layer on ablation of glacier ice. Ann Glaciol, 2: 85–91

Nicholson L, Benn D I. 2006. Calculating ice melt beneath a debris layer using meteorological data. J Glaciol, 52: 463–470

Østrem G. 1959. Ice melting under a thin layer of moraine and the existence of ice cores in moraine ridges. Geogr Ann, 41: 228–230

Pan B, Zhang G, Wang J, Cao B, Wang J, Zhang C, Geng H, Ji Y. 2012. Glacier changes from 1966–2009 in the Gongga Mountains, on the south-eastern margin of the Qinghai- Tibetan Plateau and their climatic forcing. Cryosphere, 6: 1087–1101

Paterson W S B. 1994. The Physics of Glaciers. Oxford: Elsevier Science Ltd.

Paul F, Huggel C, Kääb A. 2004. Combining satellite multispectral image data and a digital elevation model for mapping debris-covered glaciers. Remote Sens Environ, 89: 510–518

Pu J. 1994. Glacier Inventory of China VIII (the Changjiang (Yangtze) River Drainage Basin) (in Chinese). Lanzhou: Gansu Culture Publishing House. 117–129

Racoviteanu A E, Paul F, Paup B, Khalsa S H S, Armstrong R. 2009. Challeges and recommendatios in mapping of glacier parameters from space: Results of the 2008 Global Land Ice Measurements from Space (GLIMS) workshop, Boulder, Colorado, USA. Ann Glaciol, 50: 53–69

Rana B, Nakawo M, Fukushima Y, Ageta Y. 1997. Application of a conceptual precipitation–runoff model (HYCY-MODEL) in a debris-covered glacierized basin in the Langtang Valley, Nepal Himalaya. Ann Glaciol, 25: 226–231

Reid T D, Brock B W. 2010. An energy-balance model for debris-covered glaciers including heat conduction through the debris layer. J Glaciol, 56: 903–916

Reid T D, Carenzo M, Pellicciotti F, Brock B W. 2012. Including debris cover effects in a distributed model of glacier ablation. J Geophys Res, 117: D18105

Röhl K. 2008. Characteristics and evolution of supraglacial ponds on debris-covered Tasman Glacier, New Zealand. J Glaciol, 54: 867–880

Rounce D R, McKinney D C. 2014. Debris thickness of glaciers in the Everest area (Nepal Himalaya) derived from satellite imagery using a nonlinear energy balance model. Cryosphere, 8: 1317–1329

Sakai A, Fujita K. 2010. Formation conditions of supraglacial lakes on debris-covered glaciers in the Himalayas. J Glaciol, 56: 177–181

Sakai A, Nakawo M, Fujita K. 2002. Distribution characteristics and energy balance of Ice cliffs on debris-covered glaciers, Nepal Himalaya. Arct Antarct Alp Res, 34: 12–19

Sakai A, Takeuchi N, Fujita K, Nakawo M. 2000. Role of supraglacial ponds in the ablation processes of a debris-covered glacier in the Nepal Himalayas. Int Assoc Hydrol Sci Publ, 264: 119–130

Scherler D, Bookhagen B, Strecker M R. 2011. Spatially variable response of Himalayan glaciers to climate change affected by debris cover. Nature Geosci, 4: 156–159

Sekiguchi S, Tanaka Y, Kojima I, Yamamoto N, Yokoyama S, Tanimura Y, Nakamura R, Iwao K, Tsuchida S. 2008. Design principles and it overviews of the GEO grid. IEEE Syst J, 2: 374–389

Shi Y, Liu S. 2000. Estimation on the response of glaciers in China to the global warming in the 21st century. Chin Sci Bull, 45: 668–672

Shi Y, Liu C, Wang Z, Liu S, Ye B. 2005. A Concise China Glacier Inventory (in Chinese). Shanghai: Shanghai Science Popularization Press. 8–9

Song G. 1994. Movement features of Hailuogou Glacier in the Gongga Mountain. In: Xie Z, Kotlyakov V M, eds. Glaciers and Environment in the Qinhai-Xizang (Tibet) Plateau (I)—The Gongga Mountain. Beijing and New York: Science Press. 110–120

Su Z, Liu S, Wang N, Shi A. 1992. Recent fluctuations of glaciers in the Gongga Mountains. Ann Glaciol, 16: 163–167

Su Z, Song G, Wang L, Zhang W, Zhang H, Yang C, Liang D. 1985. Modern glaciers in Mt Tuomer Distric (in Chinese). In: Mountaineering and Expedition Team of Chinese Academy of Sciences, eds. Glacial and Weather in Mt Tuomuer District. Tianshan. Urumuqi: Xinjiang Renmin Press. 69–75

Suzuki R, Fujita K, Ageta Y. 2007. Spatial distribution of the thermal properties on debris-covered glaciers in the Himalayas derived from ASTER data. Bull Glaciol Res, 24: 13–22

Takeuchi Y, Kayastha R B, Nakawo M. 2000. Characteristics of ablation and heat balance in debris-free and debris-covered areaas on Khumbu Glacier, Nepal Himalayas, in the pre-monsoon season. Int Assoc Hydrol Sci Publ, 264: 53–61

Yao T, Thompson L, Yang W, Yu W, Gao Y, Guo X, Yang X, Duan K, Zhao H, Xu B, Pu J, Lu A, Xiang Y, Kattel D B, Joswiak D. 2012. Different glacier status with atmospheric circulations in Tibetan Plateau and surroundings. Nature Clim Change, 2: 663–667

Yatagai A, Arakawa O, Kamiguchi K, Kawamoto H, Nodzu M I, Hamada A. 2009. A 44-year daily gridded precipitation dataset for Asia based on a dense network of rain gauges. SOLA, 5: 137–140

Zhang Y, Fujita K, Liu S, Liu Q, Nuimura T. 2011. Distribution of debris thickness and its effect on ice melt at Hailuogou Glacier, southeastern Tibetan Plateau, using *in situ* surveys and ASTER imagery. J Glaciol, 57: 1147–1157

Zhang Y, Fujita K, Liu S, Liu Q, Wang X. 2010. Multi-decadal ice-velocity and elevation changes of a monsoonal maritime glacier: Hailuogou Glacier, China. J Glaciol, 56: 65–74

Zhang Y, Hirabayashi Y, Liu Q, Liu S. 2015. Glacier runoff and its impact for a highly glacierized catchment in the south-eastern Tibetan Plateau: past and future trends. J Glaciol, 61: 713–730

Zhang Y, Hirabayashi Y, Liu S. 2012. Catchment-scale reconstruction of glacier mass balance using observations and global climate data: Case study of the Hailuogou catchment, south-eastern Tibetan Plateau. J Hydrol, 444-445: 146–160

Zhang Y, Liu S, Ding Y. 2007. Glacier meltwater and runoff modelling, Keqicar Baqi glacier, southwestern Tien Shan, China. J Glaciol, 53: 91–98

Zhang Y, Liu S, Ding Y, Shangguan D. 2006. Preliminary study of mass balance on the Keqicar Baxi Glacier on the south slopes of Tianshan Mountains (in Chinese). J Glaciol Geocry, 28: 477–484